Mon. Not. R. Astron. Soc. **000**, 1–6 (yyyy) Printed 19 July 2013 (MN LATEX style file v2.2)

SiO Molecular Jets around young stars - A numerical perspective

B. Vaidya[1⋆], Tom Douglas[1], Paola Caselli[1], Tom Hartquist[1]
[1]*School of Physics and Astronomy, University of Leeds, Leeds LS2 9JT*

19 July 2013

ABSTRACT

Key words: MHD – methods:numerical – ISM: jets and outflows

1 INTRODUCTION

Interaction of jet with ambient medium , Class 0 sources, momentum and energy injection, High mass and low mass outflows

Observations of Outflows in CO and SiO in mm, H2 in IR, Optical jets HH objects, syncrotron emission

Molecules from jet driven or wind driven, Interesting features like EHV, low velocity component etc, list interesting outflows from Class 0

Attempts of simulations either only dynamics with analytic approaches to compare observational features, or only chemistry to estimate abundances. The reality lies in the middle!

Combine dynamics of MHD jet with molecular chemistry and comparing with observations via post-processing simulations with line radiative transfer codes.

Paper Layout

2 NUMERICAL SETUP

2.1 Numerical code and Equations

For our study, we carry out axisymmetric numerical ideal MHD simulations using the PLUTO code (Mignone et al. 2007) which is based on a conservative scheme of Godunov type. We have modified the original code to incorporate molecular cooling from self-consistent evolution of hydrogen chemistry (see Sect. 3).

In general, the MHD code considers the following set of equations. The conservation of the mass and the momentum,

$$\frac{\partial \rho}{\partial t} + (\vec{v}\cdot\nabla)\rho + \rho\nabla\cdot\vec{v} = 0 \tag{1}$$

$$\rho(\frac{\partial \vec{v}}{\partial t} + (\vec{v}\cdot\nabla)\vec{v}) = -\nabla P + \frac{1}{4\pi}(\nabla\times\vec{B})\times\vec{B} \tag{2}$$

where ρ is gas density, $\vec{v}$ the velocity vector, P the gas pressure, and $\vec{B}$ the magnetic field vector with the poloidal and toroidal components - $\vec{B}_{\rm p}, B_\phi$. Note that the forces due to gravity are neglected for this problem as the domain of interest is far away from the central object (i.e., star).

The cooling function Λ which dependents on temperature T, mass density ρ and chemical abundances $\mathbf{X}$, appears in the energy equation as a source term,

$$\frac{\partial}{\partial t}(\rho E) + \nabla\cdot\left[\rho E\vec{v} + (P + \frac{B^2}{8\pi})\vec{v}\right] - \vec{B}(\vec{v}\cdot\vec{B}) = \Lambda(\rho, T, \mathbf{X}), \tag{3}$$

where the total energy density of the flow E comprises contributions from the internal energy ϵ, the mechanical energy and the magnetic energy,

$$E = \epsilon + \frac{v^2}{2} + \frac{B^2}{8\pi\rho}. \tag{4}$$

The gas pressure in the flow is related to the density assuming an equation of state with the adiabatic index γ,

$$P = (\gamma - 1)\rho\epsilon. \tag{5}$$

The evolution of chemical abundances for each species is solved via,

$$\frac{\partial \rho\mathbf{X}_i}{\partial t} + \nabla\cdot(\rho\mathbf{X}_i\vec{v}) = \rho\mathbf{S}_i, \tag{6}$$

where $\mathbf{S}_i$ represents the net creation or destruction of a given species through chemical reactions (see Sect. 3).

The evolution of the magnetic field is governed by induction equation,

$$\frac{\partial \vec{B}}{\partial t} = \nabla\times\left(\vec{v}\times\vec{B}\right). \tag{7}$$

⋆ E-mail: B.Vaidya@leeds.ac.uk (BV)

In addition to the above set of equations the code obeys the condition of divergence-free magnetic fields, $\nabla \cdot \vec{B} = 0$, which is numerically achieved by construction since using the Powell's eight wave formulation.

2.2 Initial Condition

We model the propagation of jet as it interacts with the molecular cloud core much further from the central object, i.e., $> 1000\,\mathrm{AU}$. Further away from the central source, the downward pull of gravity plays a negligible role and the dynamics of jet is primarily governed by magnetic fields. The total magnetic field in jet is dominated by the toroidal component. This is because the poloidal field decays as z^{-2} as compared to z^{-1} for toroidal field to maintain the force balance (z is the vertical distance from source). The hoop stress due to pinch force from toroidal magnetic fields maintains the a highly collimated beam like structure for the jet.

The ambient medium with which the jet interacts primarily represents the molecular cloud core. The numerical domain is axi-symmetric and in (r,z,ϕ) cylindrical coordinates. Its extent in radial direction is 20 $R_{\rm j}$ and 100 $R_{\rm j}$ along the vertical axis, $R_{\rm j}$ being the radius of the jet. The domain is resolved by an uniform grid with 200 cells in radial and 1000 cells in vertical direction. For simplicity, we choose this medium to be unmagnetized and non-turbulent. The density in the ambient medium varies with vertical height z as, $\rho_{\rm amb} \sim (\rho_0/z^2)$ consistent with observations (Caselli 2011). The value of ρ_0 depends upon the density contrast, η, between the jet and the ambient medium. The number density in the jet is kept fixed such that the density in ambient medium lies within a range of $10^4 - 10^5 \mathrm{cm}^{-3}$. The pressure in the ambient molecular medium is set so to maintain a constant temperature of 50 K.

The jet enters into the medium through a nozzle of radius $R_{\rm jet}$ from the lower boundary (z = 0). The jet density is fixed to be $10^5 \mathrm{cm}^{-3}$ and it has a radius of 2.5×10^{15}cm $\sim$ 167 AU. The jet is injected into the domain with a typical velocity of $v_{\rm jet,0} = 100$ km/s as is the case for most low mass stellar jets specially the low velocity component. The constant jet velocity is superimposed with periodic pulsation of the form,

$$v_{\rm jet} = v_{\rm jet,0}(1.0 + A\, sin(2.0\pi t/T_{\rm p})) \qquad (8)$$

where the amplitude A is 0.25 and time period $T_{\rm p}$ = 70 years. The pressure at the surface of the jet is 10^{-10}dyne cm^{-2} corresponding to a temperature of $T_{\rm jet} \sim 4 \times 10^3\, K$. Inside the jet beam, a radial variation of thermal and magnetic pressure is adopted to maintain a magnetostatic equilibrium. We adopt the same radial profiles used by Stone & Hardee (2000) for all our runs. Based on these profiles, the toroidal magnetic field is assumed to be zero at the axis and achieves a maximum at some radius, $r_{\rm m}$ inside the jet. The maximum value, $B_{\phi,\rm m}$, depends on the plasma β which is a parameter used for our study along with the density contrast η.

In order to consistently model the SiO emission arising from shocks as this jet interacts with the medium, we evolve the dynamics along with chemistry and cooling prescribtions. They are described in details in the next section.

3 CHEMISTRY AND COOLING

3.1 Power law cooling

3.2 Atomic Cooling

3.3 Tabulated Cooling

3.4 Molecular Cooling

The evolution of molecular, atomic and ionized hydrogen is governed by equations listed in Table 1. In this cooling mode, these equations are evolved at each times using temperature dependent rates mentioned in the table along with their source. The code tracks the formation and destruction of three quantities viz., X(HI), X(H_2) and X(HII) with a constraint that sum of all three should be unity. Further, these abundances are used to update the cooling function $\Lambda(n, T, \mathbf{X})$ to consistently derive the temperature for next advection step.

4 RADIATIVE TRANSFER

Radiative transfer modeling used for post processing.

4.1 The radiative transfer code

The radiative transfer program used is LIME (LIne Modeling Engine; Brinch & Hogerheijde 2010), which calculates line intensities based on a weighted sample of randomly chosen points in a continuous 3D model. The method of selecting these points is given in section 4.2. At each of these points, the density of the main collision partner (equivalent amount of H_2, given by n(H_2)+ 0.5 n(H)), gas and dust temperatures, velocity, molecular abundances and unresolved turbulent velocity are specified. These points are then smoothed by Lloyd's algorithm (Lloyd 1982) in order to minimise the variation in distance between points whilst keeping the same underlying distribution. These points are then connected by Delaunay triangulation and it is between the points connected by this method that photon are allowed to propagate (fig. 10). The level populations of the selected molecules are calculated at each of these points from collisional and radiative (de)excitation and the local radiation field is calculated. This is repeated 20 times with the populations of each level converging towards a single value. This number of iterations is sufficient for the signal to noise ratio of the level populations (as defined in Brinch & Hogerheijde 2010) to exceed 1000 for 99% of the points, ensuring that the simulation has converged on a stable level population. After 20 iterations the model is ray-traced in order to produce synthetic brightness maps. The average of ten separate runs was taken to minimise the artefacts in the output images, resulting from the grid construction (Fig. 3).

4.2 Grid construction

In order to construct the grid, candidate points are randomly selected from the volume to be simulated. These candidates then have their equivalent H_2 number density, and the number density of SiO, compared against those of a reference point in order to decide if the candidate point is to be used

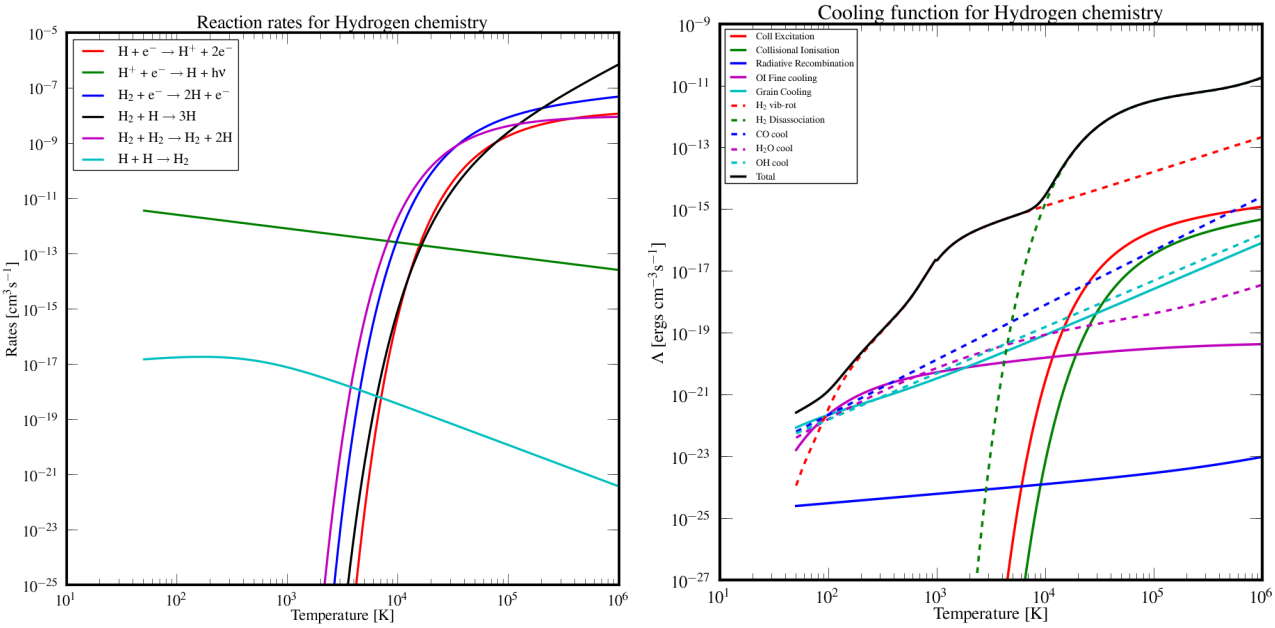

Figure 1. Variation of H_2 chemistry reaction rates, k_i and cooling function $\Lambda(n, T, \mathbf{X})$ with temperature for the initial state (see Sect. 3.4)

Table 1. Summary of the chemistry reaction set. T is the temperature in Kelvin, $T_{\rm eV}$ is the temperature in electron-volts, $T_5 = T/1\times10^5$ and T_2 = T/100

No.	Reaction	Rate Coefficient ($\rm cm^3 s^{-1}$)	Reference [a]
1.	$H + e^- \rightarrow H^+ + 2e^-$	$k_1 = 5.85\times10^{-11}\ T^{0.5}\ \exp(\text{-}157{,}809.1/T)/(1.0 + T_5^{0.5})$	1
2.	$H^+ + e^- \rightarrow H + h\nu$	$k_2 = 3.5\times10^{-12}(T/300.0)^{-0.8}$	2
3.	$H_2 + e^- \rightarrow 2H + e^-$	$k_3 = 4.4\times10^{-10}T^{0.35}\exp(-102{,}000.0/T)$	3
4.	$H_2 + H \rightarrow 3H$	$k_4 = 1.067\times10^{-10}T_{\rm eV}^{2.012}(\exp(4.463/T_{\rm eV})^{-1}((1. + 0.2472T_{\rm eV})^{3.512})^{-1}$	4
5.	$H_2 + H_2 \rightarrow H_2 + 2H$	$k_5 = 1.0\times10^{-8}\exp(-84,100/T)$	2
6.	$H + H \xrightarrow{\rm dust} H_2$	$k_6 = 3.0\times10^{-17}\sqrt{T_2}(1.0 + 0.4\sqrt{T_2 + 0.15} + 0.2T_2 + 0.8T_2^2)$	5

[a] REFERENCES – (1) Cen (1992) [Eq. 26a]; (2) Woodall et al. (2007) [UMIST Database] (3) Galli & Palla (1998) [Eq. H17]; (4) Abel et al. (1997) [Tab. 3 Eq. 13]; (5) Hollenbach & McKee (1979) [Eq. 3.8]

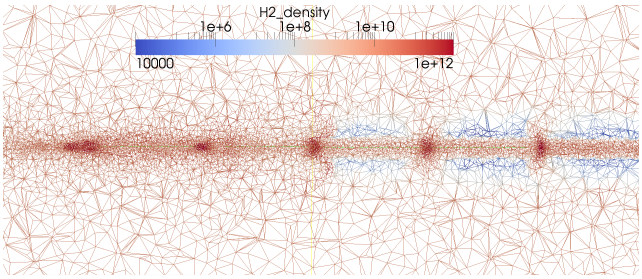

Figure 2. A plot of the points selected by the gridding process and the paths down which photons can propagate for points in the r,z plane. The points are color coded by the density distribution (in $\rm m^{-3}$, as used in LIME) and are more concentrated in the high density knots.

in the grid or not. Candidate grid points are selected at random in a cylindrical coordinates that is linearly spaced in z and θ and logarithmically spaced in r. For each point to be selected, a random number α is drawn from the semi-open set $[0, 1)$ as a threshold. After selection of random coordinates, the H_2 density and SiO density at the candidate point (n and m, respectively) are compared against the densities of a reference point in the un-perturbed ambient medium multiplied by $\frac{4\eta}{5}$ (n_0 and m_0). If $\alpha < \left(\frac{n}{n_0}\right)^{0.3}$ or $\alpha < \left(\frac{m}{m_0}\right)^{0.3}$ then the point is selected for use. Otherwise another r, θ, z co-ordinate is selected and it becomes the candidate point. In addition to this method of selection, 5% of the points are linearly distributed in x, y and z with no bias with regards to density or abundance. This provides a minimum level of sampling for the large low density regions in the outer parts of the simulated volume. See fig. 3 for an example of the points distribution in r, z. The function comparing the candidate point to the reference point and the candidate point distribution were selected empirically to sample all scales while ensuring that the majority of points are located in the inner disc where the density is higher.

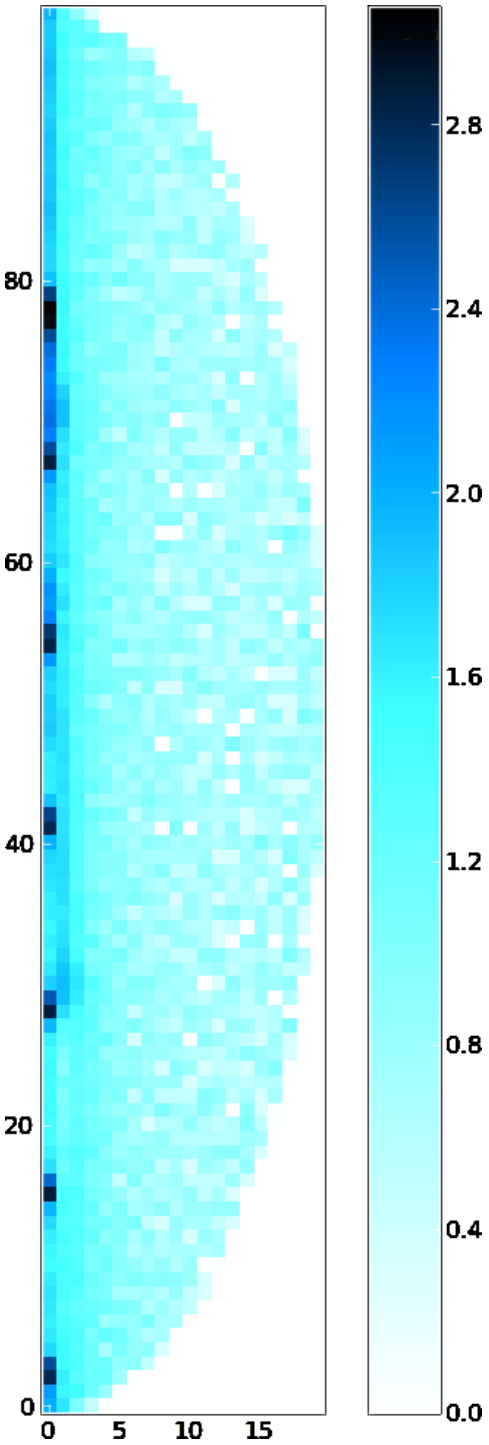

Figure 3. A 2D histogram of the point distribution throughout the model. The disc and envelope can be seen as two separate entities which have to be sampled using different point distributions.

4.3 SiO abundance

Need refs for this!!The amount of SiO is determined by the local velocity and temperature. The fractional abundance is given by the equation:

$$log(X) = -2.48 \times 10^{-8} v^5 + 5.50 \times 10^{-6} v^4 - 4.28 \times 10^{-4} v^3 + 1.24 \times 10^{-2} v^2 + 2.52 \times 10^{-2} v - 1.20 \times 10^{1}$$

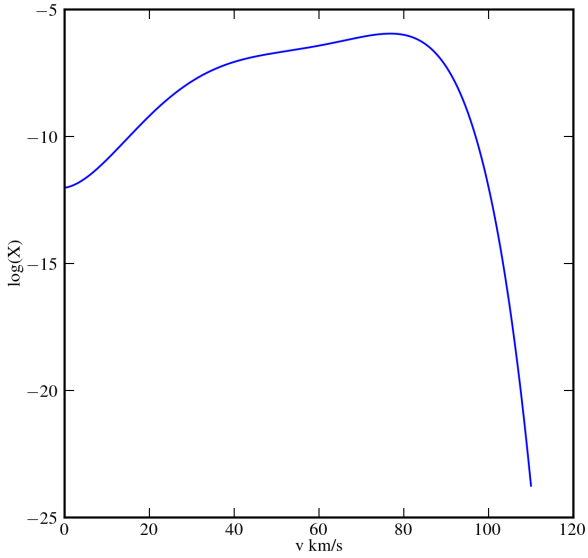

Figure 4. The polynomial used to calculate an abundance of SiO as a function of local velocity.

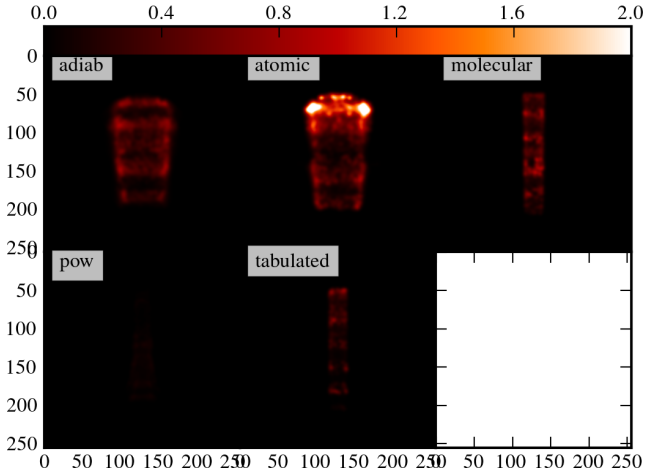

Figure 8. A plot of the integrated SiO J2-1 emission from 5 models, each using a different method to calculate cooling and all with η=10 β=10.

where v is in kilometres per second. In addition to this if the temperature at the point is greater than 92,000K (the temperature of the Si-O bond disassociation energy) the abundance is reduced to 10^{-30}.

5 RESULTS

Table 1 – Parameter runs with changing β (magnetic fields) and η (density contrast) for cooling
Results should have Peak Intensity after convolution., FWHM at tip of bow shock.
Our reference run – β = 10.0, η = 2.0, with cooling and velocity dependent SiO Abundance.
Figure 3 – Output from MHD simulations (Reference run).

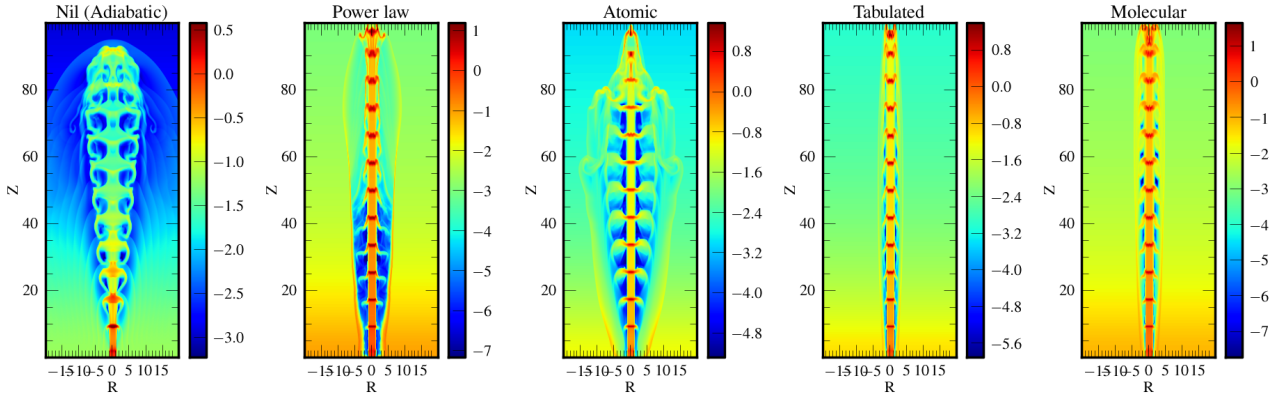

Figure 5. Jet Volume Density for different cooling modes with $\eta = 10$ and $\beta = 10$.

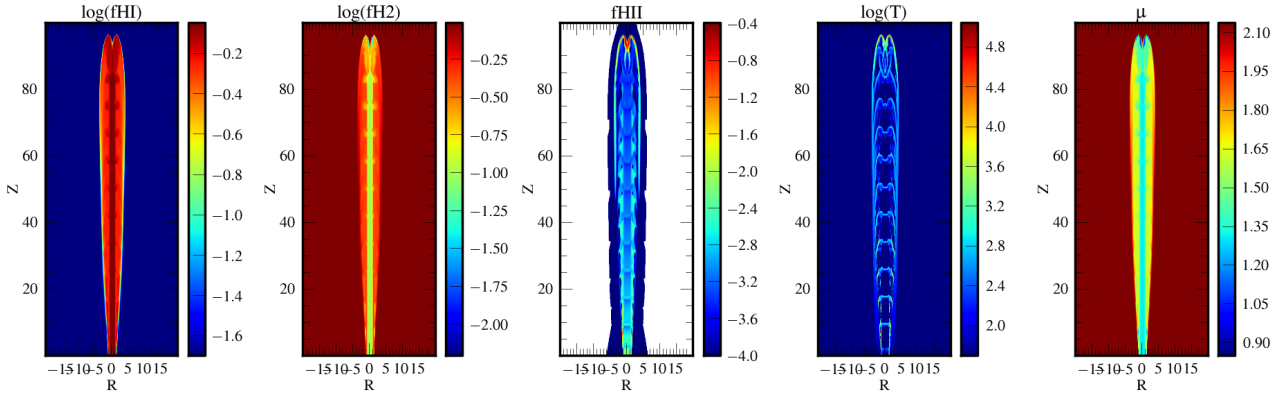

Figure 6. Fraction of hydrogen species in the run with molecular cooling having $\eta = 5$ and $\beta = 10$.

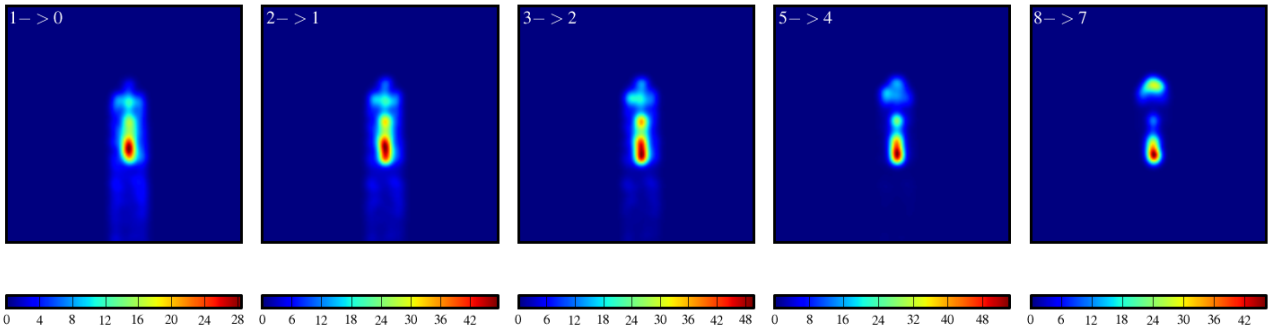

Figure 7. SiO emission from different line transitions for the run with molecular cooling having $\eta = 3$ and $\beta = 10$.

Table 2. Summary from parameter runs

Run	Cooling Mode	η	β	Peak Intensity [K]	FWHM at Bow Shock
adi1010	Nil (Adiabatic)	10	10		
pow1010	Power law	10	10		
atm1010	Atomic	10	10		
atm101	Atomic	10	1		
atm210	Atomic	2	10		
tab1010	Tabulated	10	10		
tab210	Tabulated	2	10		
mol1010	Molecular	10	10		
mol510	Molecular	5	10		

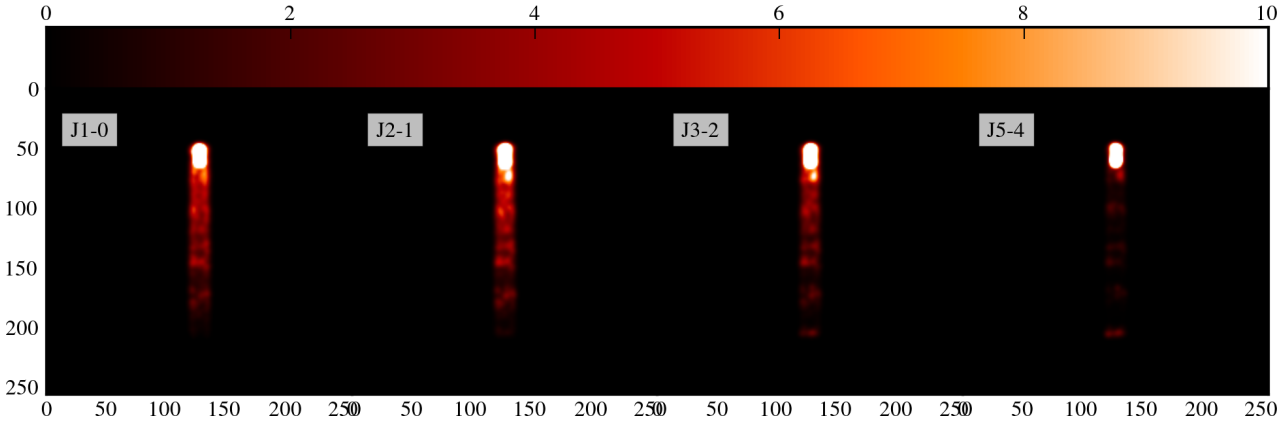

Figure 9. The integrated intensity of 4 SiO transitions in the tabulated cooling model in the η=2 β=10 model.

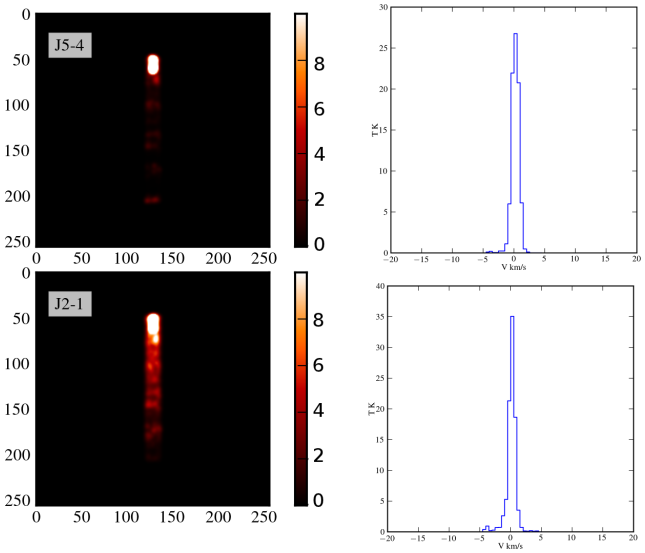

Figure 10. The Integrated emission and spectra at he bow shock for 2 transitions of the tabulated cooling model for η=2 β=10 (spectra taken from y=50, x=128).

Figure 4 – Output from Rad Transfer (Reference run). Integrated Intensity Maps for different transitions for three different cooling prescribtions. (TODO : TOM)
Figure 5 – Spectra for the reference runs all transitions. (TODO : TOM)
Figure 6 – PV diagrams (TODO : TOM) for one transition in two directions. Figure 7 – Angle of Inclination dependence

6 DISCUSSION

Effects of varying η
Lower η gives better emission.

Importance of cooling prescriptions

Bulk of emission comes from cooling instabilities.

Spectra and PV Digrams

Line - withs $\sim$ 15-25 km s^{-1}. Wedge shaped PV diagrams a signature feature of jet driven molecular outflows.

Comparison with Observed results

Different line transition trace different components of SiO emission. The low level transitions trace the region where the jet interacts with molecular medium. The clumpy nature in its emission is from the turbulent nature of its interaction. The higher transitions trace a much more collimated region along with the terminal shock. As seen by Chandler & Richer 2001 and Hirano 2006.

Limitations

7 ALMA VIEW

ALMA view of the reference run and stress of applying our synthetic techniques to study the molecular outflows in more details.
Figure 6. for ALMA –

8 CONCLUSION

We are the best in modelling SiO outflows.

REFERENCES

Abel T., Anninos P., Zhang Y., Norman M. L., 1997, New A, 2, 181
Brinch C., Hogerheijde M. R., 2010, A&A, 523, A25
Caselli P., 2011, in Cernicharo J., Bachiller R., eds, IAU Symposium Vol. 280 of IAU Symposium, Observational Studies of Pre-Stellar Cores and Infrared Dark Clouds. pp 19–32
Cen R., 1992, ApJS, 78, 341
Galli D., Palla F., 1998, A&A, 335, 403
Hollenbach D., McKee C. F., 1979, ApJS, 41, 555
Lloyd S., 1982, Information Theory, IEEE Transactions on, 28, 129
Mignone A., Bodo G., Massaglia S., Matsakos T., Tesileanu O., Zanni C., Ferrari A., 2007, ApJS, 170, 228
Stone J. M., Hardee P. E., 2000, ApJ, 540, 192
Woodall J., Agúndez M., Markwick-Kemper A. J., Millar T. J., 2007, A&A, 466, 1197